Cerebral Cortex January 2007;17:81-91
doi:10.1093/cercor/bhj126
Advance Access publication February 8, 2006

Correlation Between Axonal Morphologies and Synaptic Input Kinetics of Interneurons from Mouse Visual Cortex

Daniella Dumitriu[1], Rosa Cossart[1,3], Josh Huang[2] and Rafael Yuste[1]

[1]Howard Hughes Medical Institute, Department of Biological Sciences, Columbia University, New York, NY 10027, USA and [2]Cold Spring Harbor Laboratory, Cold Spring Harbor, NY 11724, USA
[3]Current address: Institut de Neurobiologie de la Mediterranée, Institut National de la Santé et de la Recherche Médicale, U29, 13673 Marseille, France

Neocortical interneurons display great morphological and physiological variability and are ideally positioned to control circuit dynamics, although their exact role is still poorly understood. To better understand this diversity, we have performed a detailed anatomical and physiological characterization of 3 subtypes of visual cortex interneurons, isolated from transgenic mice which express green fluorescent protein in somatostatin, parvalbumin, and neuropeptide Y positive neurons. We find that these 3 groups of interneurons have systematic differences in dendritic and axonal morphologies and also characteristically differ in the frequencies, amplitude, and kinetics of the spontaneous excitatory and inhibitory synaptic currents they receive. Moreover, we detect a correlation between the kinetics of their synaptic inputs and quantitative aspects of their axonal arborizations. This suggests that different interneuron types could channel different temporal patterns of activity. Our results also confirm the importance of the axonal morphology to classify interneurons.

Keywords: cortex, EPSP, GABA, GFP, IPSP

Introduction

Although γ-aminobutyric acid (GABA)ergic interneurons comprise the minority of neocortical neurons, they are responsible for the largest degree of morphological, electrophysiological, and neurochemical heterogeneity in the cortex (Ramón y Cajal 1899; Lorente de No 1922; Fairen and others 1984; Somogyi and others 1998; Gupta and others 2000). This rich diversity suggests that the inhibitory components of the cortical circuitry play a critical role in network computation.

Characterization of cortical interneurons has been a major challenge due to their impressive multiparametric diversity (Parra and others 1998; Mott and Dingledine 2003). To understand interneuronal function, it is necessary to identify interneurons and characterize whether or not they belong to particular classes. This is not an academic exercise because, like in the retina (Sterling 1990), each neuronal class could implement a distinct circuit function. Despite advances in recent years, a meaningful classification scheme of these cells has nonetheless proved difficult (Mott and Dingledine 2003). Parra and others (1998) argued that interneurons cannot be meaningfully classified because their anatomical and physiological diversity could represent a continuum (Maccaferri and Lacaille 2003; Baraban and Tallent 2004; Jonas and others 2004). In the tradition of the Golgi anatomists (Ramón y Cajal 1899; Lorente de No 1922; Fairen and others 1984), other groups have proposed different classifications of interneurons, based on morphological or physiological parameters (Freund and Buzsaki 1996; Gonchar and Burkhalter 1997; Kawaguchi and Kubota 1997; Somogyi and others 1998; Gupta and others 2000; Wang and others 2002; Klausberger and others 2003). Nevertheless, we are still far from an universally accepted interneuron taxonomy, and the question still remains open (for documents of the recent Petilla meeting devoted to this topic, see http://www.columbia.edu/cu/biology/faculty/yuste/petilla/index.html).

Whereas many interneuron classifications have focused on the morphology or various aspects of their output (i.e., the firing pattern and the postsynaptic potentials they generate on their targets), Cossart and others (2006) found an intriguing correlation between the morphology and synaptic input kinetics of hippocampal interneurons. To explore if those findings extend to neocortex, we used cluster analysis to examine the correlation between the morphology and the inputs of neocortical interneurons (i.e., the postsynaptic currents [PSCs] they receive). To study this, we took advantage of the growing number of green fluorescent protein (GFP) transgenic mouse strains labeling homogenous populations of interneurons that express specific markers, such as parvalbumin (PV), neuropeptide Y (NPY), and somatostatin (SOM). We made brain slices from the visual cortex of these animals and used targeted whole-cell recordings from fluorescently labeled cells to record their synaptic currents and also fill them with biocytin for post hoc reconstruction of their morphologies. Our quantitative analysis supports the existence of distinct clusters of interneurons. We find a high degree of correlation between the neurochemical content, the morphology, and the excitatory postsynaptic potentials or inhibitory postsynaptic potentials of PV-, NPY-, and SOM-labeled interneurons, with a surprising degree of correlation evolving specifically from axonal morphologies. The correlation between axonal morphologies and the kinetics of PSCs received by the cell is striking as it suggests a highly systematic network with both pre- and postsynaptic component specificity. Our results provide a potential mechanism for how distinct interneuronal circuits could temporally control distinct parts of pyramidal cell dendritic arbors and participate at distinct phases of network rhythms (Klausberger and others 2003).

Materials and Methods

Animals

SOM mice were from an original albino strain (Oliva and others 2000), whereas PV and NPY mice were derived from C57/Bl6 founders (Roseberry and others 2004). Backcrossings were performed with wild type C57/Bl6 mice. For PV mice, bacterial artifical chromosome (BAC) clones containing the mouse paravalbumin (Pv) genes were identified from the Roswell Park Cancer Institute-23 library (Research Genetics). A BAC clone containing the entire Pv gene and 140 kb of upstream and 30 kb of downstream regions was used for BAC modification. A DNA fragment containing enhanced green fluorescent protein (EGFP) cDNA and the phosphoglycerate kinase poly adenylation

sequence was inserted at the translation initiation codon of the PV gene. Circular BAC DNA was injected by conventional methods to generate BAC transgenic mice. In the transgenic line used in this study, B13, EGFP was selectively expressed in approximately 50% Pv-positive interneurons in neocortex, including visual cortex. The developmental time course of EGFP expression resembled that of Pv assay by immunostaining. Detailed procedure and characterization will be published elsewhere.

Electrophysiology

Acute coronal slices of mouse visual cortex were prepared from postnatal days 14 to 23 mice in accordance with Columbia University and National Institute of Health guidelines for animal use in biomedical research. Most animals were P15–16, and no clear differences were found among ages. Animals were anesthetized with 0.05 cc of a mixture of ketamine and zylazine (50 and 2.5 mg/ml). After decapitation, brains were rapidly removed and placed in ice-cold cutting solution containing in millimolar: 3 KCl, 1.5 NaH_2PO_2, 27 $NaHCO_3$, 222 sucrose, 1 $CaCl_2$, 4 $MgSO_4$, bubbled with 95%O_2–5%CO_2 to pH 7.4. Brains were cooled for a minimum of 2 min, and 300 μM slices of visual cortex were cut with a Vibratome (Leica VT1000S). Slices were then placed in room temperature artificial cerebral spinal fluid (ACSF) containing in millimolar: 126 NaCl, 3 KCl, 1.1 NaH_2PO_2, 26 $NaHCO_3$, 1 dextrose, 2 $CaCl_2$, 1 $MgSO_4$, bubbled with 95%O_2–5%CO_2 to pH 7.4. After 1 h, slices were individually moved to a recording chamber maintained at 30–33 °C and continuously perfused with oxygenated ACSF.

Interneurons from all layers in which they were observed (except layer I) were identified based on GFP fluorescence of their somata when imaged with fluorescence. The desired cell was then visualized with differential interference contrast (DIC) optics using an upright Olympus microscope (BX50WI). Whole-cell voltage clamp recordings were done using electrodes of resistances ranging between 6 and 10 MΩ and internal solution containing in millimolar: 135 Cs-gluconate, 10 MgCl2, 0.1 CaCl2, 1 ethylene glycol tetra acetic acid, 10 4-2-hydroxyethyl-1-piperazineethanesulfonic acid, 0.4% biocytin, and pH 7.25. Spontaneous activity was recorded at −60, +10 mV, or both for 52 cells (19 PV, 20 NPY, 13 SOM). Inward currents at −60 mV were determined to be due to alpha-amino-3-hydroxy-5-methyl-4-isoxazole propionic acid (AMPA) and/or kainate, as they were completely eliminated with 12.5 μM 6-cyano-7-nitroquinoxaline-2,3-dione (CNQX), whereas outward currents were determined to be due to $GABA_A$, as they were eliminated by a mixture of 100 μM picrotoxin. For a subset of cells (5 PV, 6 NPY, 6 SOM), 1 mM tetrodotoxin (TTX) was added following the recording of spontaneous activity. Miniature activity was recorded at both −60 and +10 mV.

Signals were fed to an EPC10 amplifier (Heka, Southboro, MA) and recorded on a PC using Pulse (Heka) or to a Dagan amplifier (BVC 700A, Dagan Instruments, Minneapolis, MN) and recorded on a MacIntosh using Superscope (GW Instruments, Somerville, MA). Access resistances were approximately ~10 MΩ and were not allowed to vary by more than 20% during the recording.

Electrophysiology Analysis

All physiological data were analyzed using MiniAnalysis 5.6 (Synaptosoft, Decatur, GA). For each condition (spontaneous and miniature excitatory postsynaptic currents [EPSCs] and inhibitory postsynaptic currents [IPSCs]), a minimum of 300 events was manually detected for digital averaging using 2 rpm above noise for threshold (noise ranged between 1 and 3 rpm). Amplitudes, 10–90% rise times, and single exponential decay taus were measured for each digital average. The frequency was determined by dividing the number of detected events by the duration in which they had occurred.

Morphological Reconstructions

Slices were processed as in Esclapez and others (1997). Following electrophysiological recordings, the slices were immediately placed in 4% paraformaldehyde in 0.12 M phosphate buffer (PB) and kept at 4 °C overnight. Slices were then cryoprotected in 20% sucrose in 0.12 M PB for 2–8 h and frozen on dry ice in tissue freezing medium (catalog number H-TFM, Triangle Biomedical Sciences, Durham, NC).

Upon defrosting, slices were rinsed in 0.12 M PB 3 times and pretreated with 1% hydrogen peroxide in 0.12 M PB for 30 min under agitation at room temperature. The tissue was then rinsed in 0.02 M potassium phosphate saline (KPBS) and incubated in avidin-biotin-peroxidase complex (catalog number PK-6100, Vector Laboratories, Inc., Burlingame, CA) overnight under agitation at room temperature (10 μl solution A and 10 μl solution B per 1 ml of 0.02 M KPBS and 0.3% Triton-X).

Slices were rinsed in 0.02 M KPBS 3 times and incubated in 0.7 mg/ml 3,3′-diaminobenzidine, 0.2 mg/ml urea hydrogen peroxide, 0.06 M Tris buffer (catalog number D-4293, Sigma-Aldrich, St. Louis, MO) in 0.02 M KPBS for 5–15 min. Upon completed 3,3′-diaminobenzidine reaction, the slices were rinsed in 0.02 M KPBS and mounted in Vectashield mounting medium (catalog number H-1000, Vector Laboratories, Inc.).

Stained cells were visualized with DIC optics using an Olympus inverted microscope (IX70), and 18 neurons (6 PV, 7 NPY, 5 SOM) were traced in 3 dimensions using the Neurolucida workstation. All drawings were done under a 60 × 1.40 numerical aperture objective in combination with the additional ×1.5 magnification of the microscope.

Morphological Variables

Drawn neurons were rated on 98 morphological parameters using the analytic tools of NeuroExplorer in combination with further analysis in Excel and MatLab. We did not discriminate on chosen parameters but rather tried to describe each cell as in-depth as the program allowed. Variables described soma, dendrites, axon, and the relationship between dendritic and axonal arbors (see Supplementary Table 1). A cross-correlation matrix was then performed, and variables correlated more than 80% ($P < 0.05$) with 1 or more other variables were eliminated except in cases were the correlation was between logically unrelated parameters (e.g., when a dendritic parameter was correlated with an axonal parameter). Sixty-one variables remained.

Cluster Analysis and PCA

Cluster analysis for morphological and physiological data, respectively, was conducted using Statistica's algorithm (Ward's method, Euclidean distances). In order to extract the variables most responsible for the clusters, factor analysis using the principal component analysis (PCA) method was performed on the same data. Variables more than 70% correlated with the 1st factor were extracted, resulting in 9 morphological and 4 physiological parameters. PCA was also performed on the pooled morphological and physiological data, resulting in 8 morphological and 4 physiological parameters being more than 70% correlated with the 1st factor. All individual parameters were the same as in the unpooled data with "number of dendrites" not present in the pooled data.

Results

Three strains of GFP transgenic mice were used, labeling 3 different populations of interneurons: PV (see Methods), NPY (Roseberry and others 2004), and SOM (Oliva and others 2000). In all 3 strains, GFP-labeled neurons could be visualized by epifluorescence in primary visual cortex. Neurons were targeted for whole-cell recordings and spontaneous and miniature PSCs were recorded in voltage clamp in the presence of intracellular cesium (see Methods). Cells were filled with biocytin to allow for post hoc morphological identification (see Fig. 1).

Morphological Differences among Neurochemically Identified Interneurons

We sought to classify our database according to a multidimensional morphological analysis. For this purpose, 18 cells (6 PV, 7 NPY, 5 SOM) were reconstructed in 3 dimensions. For each neuron, 98 morphological variables were measured, describing their location, the morphometric properties of their somata, dendrites, and axons as well as the relationship between dendritic and axonal arbors (see Supplementary Table 1). To remove redundancy, following a cross-correlation matrix, variables that were more than 80% correlated ($P < 0.05$) with 1 or more other variable were eliminated. Sixty-one variables remained as being significantly less correlated with each other.

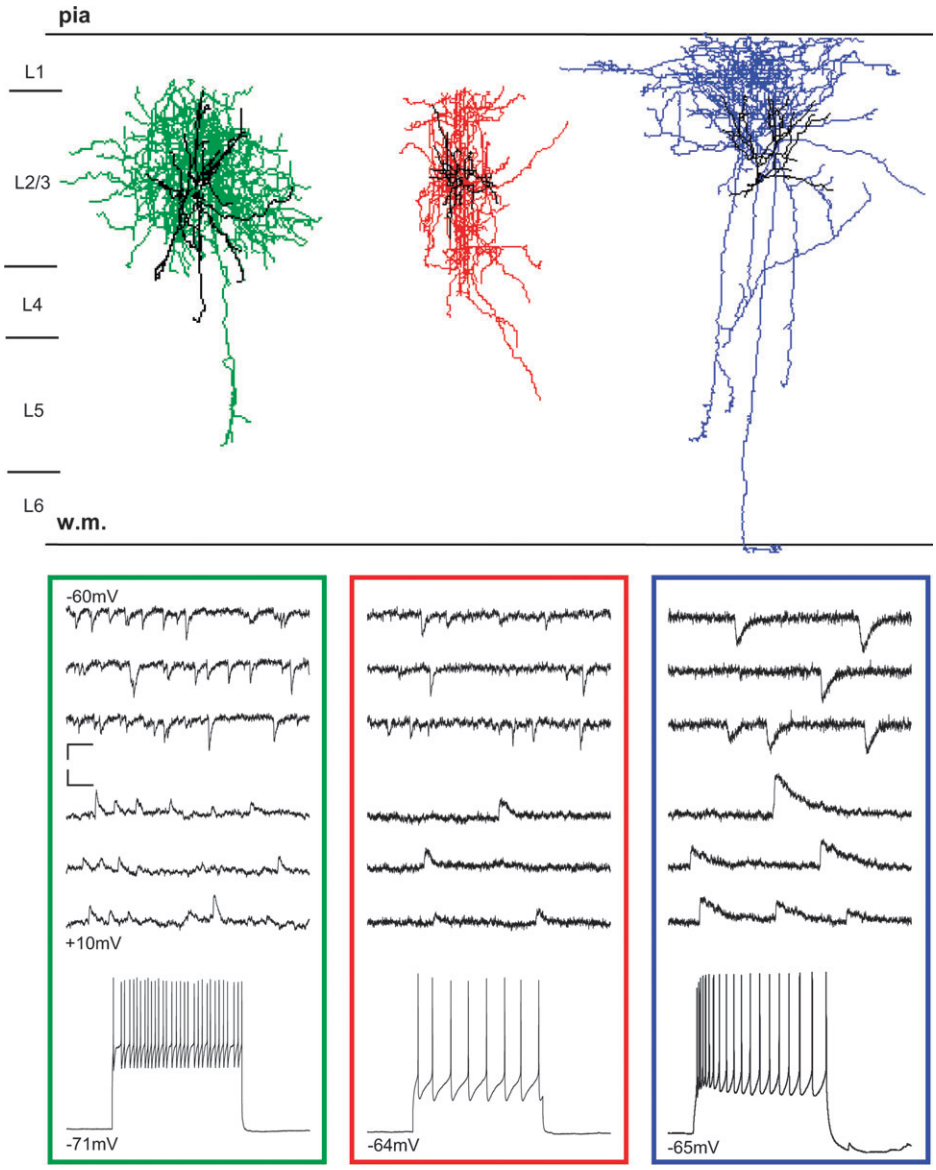

Figure 1. Anatomical and physiological characterization of PV, NPY, and SOM interneurons. Neurons were injected with biocytin during recordings and following post hoc identification reconstructed in 3 dimensions. Top: representative examples of a layer II interneuron from each group are shown here. Somata and dendrites are represented in black, whereas axons are color-coded: green for PV, red for NPY, and blue for SOM. This color scheme will be maintained for all figures. Layer boundaries marked with left bars. Bottom: representative voltage clamp recordings at –60 and +10 mV are shown for each group. Scale bars for EPSCs and IPSCs: 15 pA and 20 ms. Representative firing patterns are also shown for each group. Scale bars for each trace: 10 mV and 100 ms.

Cluster analysis was performed using these 61 variables (Fig. 2; Ward's method, Euclidean distances). All cells clustered separately into 3 clusters, in accordance with their neurochemical content, with the exception of 1 NPY cell that clustered with the PV group. Though separated by more than 30% of the maximal linkage difference, PV and NPY cells seem to belong to the same superfamily and show an almost equal linkage distance to SOM cells.

These data demonstrated that the 3 neurochemically identified groups of neocortical interneurons have systematic differences in their morphologies.

Synaptic Input Differences Identified among Interneuron Types

Synaptic inputs were characterized for each cell by computing an average of the frequency, amplitude, and onset and offset kinetics of spontaneous EPSCs and IPSCs. Spontaneous EPSCs were recorded in voltage clamp at the reversal potential for GABAergic currents (–60 mV); they were mediated by AMPA/kainate receptors because they were completely eliminated by 12.5 μM CNQX. Spontaneous IPSCs were recorded at the reversal potential for glutamatergic events (+10 mV) and were indeed mediated by $GABA_A$ receptors because they were blocked by 100 μM picrotoxin (Fig. 1). For each cell, approximately 300 EPSCs and IPSCs were digitally averaged, and for each EPSC and IPSC average, the 10–90% rise time and amplitude were measured. All decay times of digital averages were fitted to monoexponential time constants (taus) for the purpose of comparison.

All the 8 above-mentioned parameters were assessed for 39 cells (14 PV, 14 NPY, 11 SOM) and used for physiological cluster analysis (Fig. 3). With the exception of 2 PV cells, which

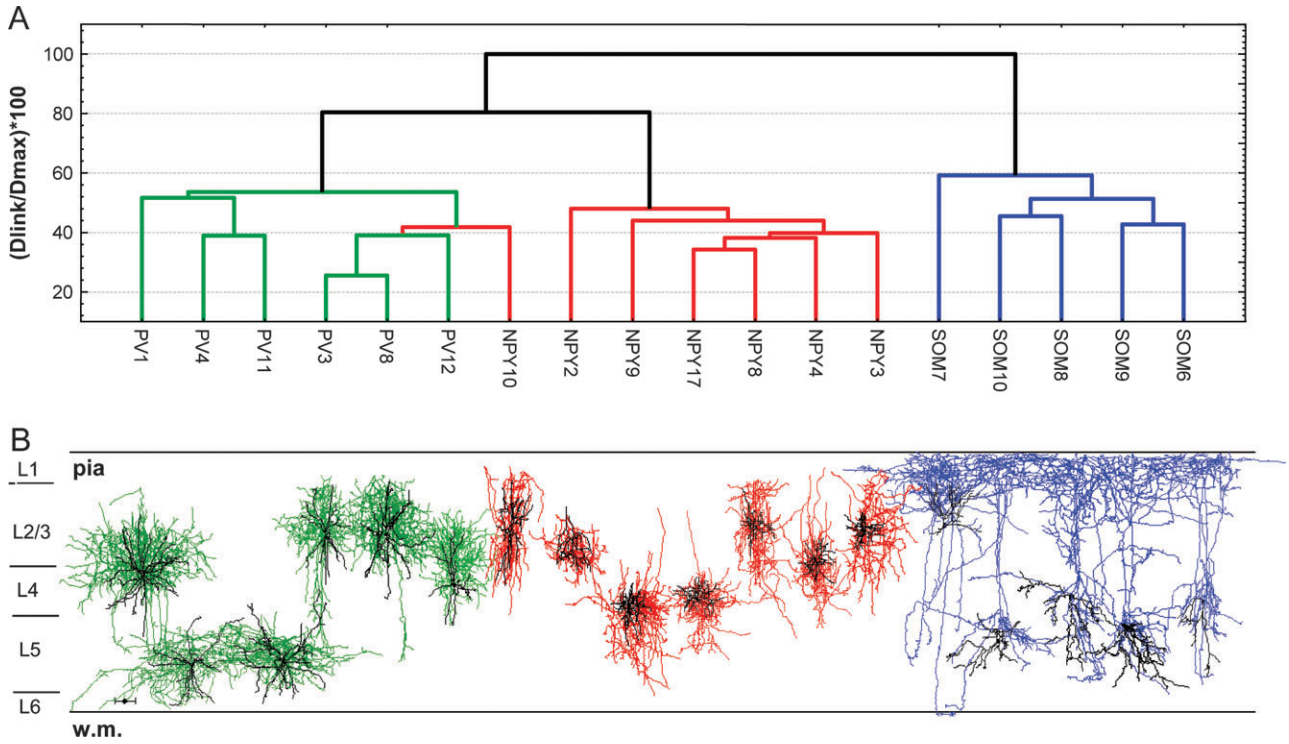

Figure 2. Morphological cluster analysis. (*A*) Cluster analysis tree representing 61 variables from 18 reconstructed interneurons. Each branch is color-coded according to the cell type that it represents. (*B*) Three-dimensional reconstructions of the interneurons entered into the cluster analysis. Neurons are placed in the order that they appear in the cluster analysis tree. Somas and dendrites are shown in black, whereas axons are shown in color according to the group they belong to. Neurons are placed vertically in accordance with their cortical layer location. Layer boundaries marked with bars. Scale bar: 100 μm.

clustered with the NPY group, synaptic input parameters also separated the 3 neurochemically identified groups of neocortical interneurons, generating the same classification as obtained with morphological parameters. Interestingly, not only did the physiological clustering separate the cells according to their neurochemical content, but also it preserved the basic relationship between groups, predicting that PV and NPY cells belonged to the same superfamily with an equal individual distance to SOM cells.

Differences in Miniature Potentials among Interneuron Types

We examined if our classification using spontaneous PSCs would hold true for miniature events as well. Following our recordings in normal conditions, 1 μM TTX was bath applied to 5 PV, 6 NPY, and 6 SOM cells. Rise time, decay tau, amplitude, and frequency of events were obtained for miniature EPSCs and IPSCs in the same way as for the spontaneous activity. Cluster analysis of the resulting 8 new parameters for the 17 cells showed a similar tree as the one obtained with spontaneous PSCs (Fig. 3*D*), with the subgroups dividing according to their neurochemical content, 1 PV cell clustering with the NPY group, and PV and NPY cells belonging to the same superfamily.

Axonal Morphology Alone can Predict Interneuron Cell Class

To examine which morphological variables were the most important predictors of synaptic input physiology in a given cell, we divided the 61 morphological variables into 3 subgroups—somatic, dendritic, and axonal—and 3 independent cluster analyses were performed. The 2 variables that described the relationship between dendritic and axonal arbors were included in both the dendritic and axonal subgroups.

We found that the somatic morphology was a very poor predictor of cell class, whereas dendritic and axonal morphologies were both able to divide the cells into the neurochemically predicted groups (Fig. 4). However, an analysis based on axonal morphology alone was able to maintain the relative distance between the families, whereas clustering based on dendritic arbor properties placed PV cells in the same superfamily as SOM cells. We concluded that axonal morphometric features are the strongest morphological predictors of interneuron families.

Morphological Predictors of Interneuron Class

Our results indicated that morphological variables and physiological variables must be characteristic to each of the 3 interneuron classes because they independently gave rise to similar clustering of cells. We further determined the individual morphological parameters that gave rise to the clustering. To identify these key variables, we performed factor analysis using PCA on morphological and physiological variables individually and combined. We then extracted all variables that correlated by more than 70% with the 1st principal component (see Methods). This led to 9 morphological and 4 physiological parameters. A correlation matrix was then computed for those variables, to ascertain the exact relationships between morphology and physiology (see Table 1). From this matrix, the variables with the highest scores were more carefully characterized with respect to the 3 groups of interneurons.

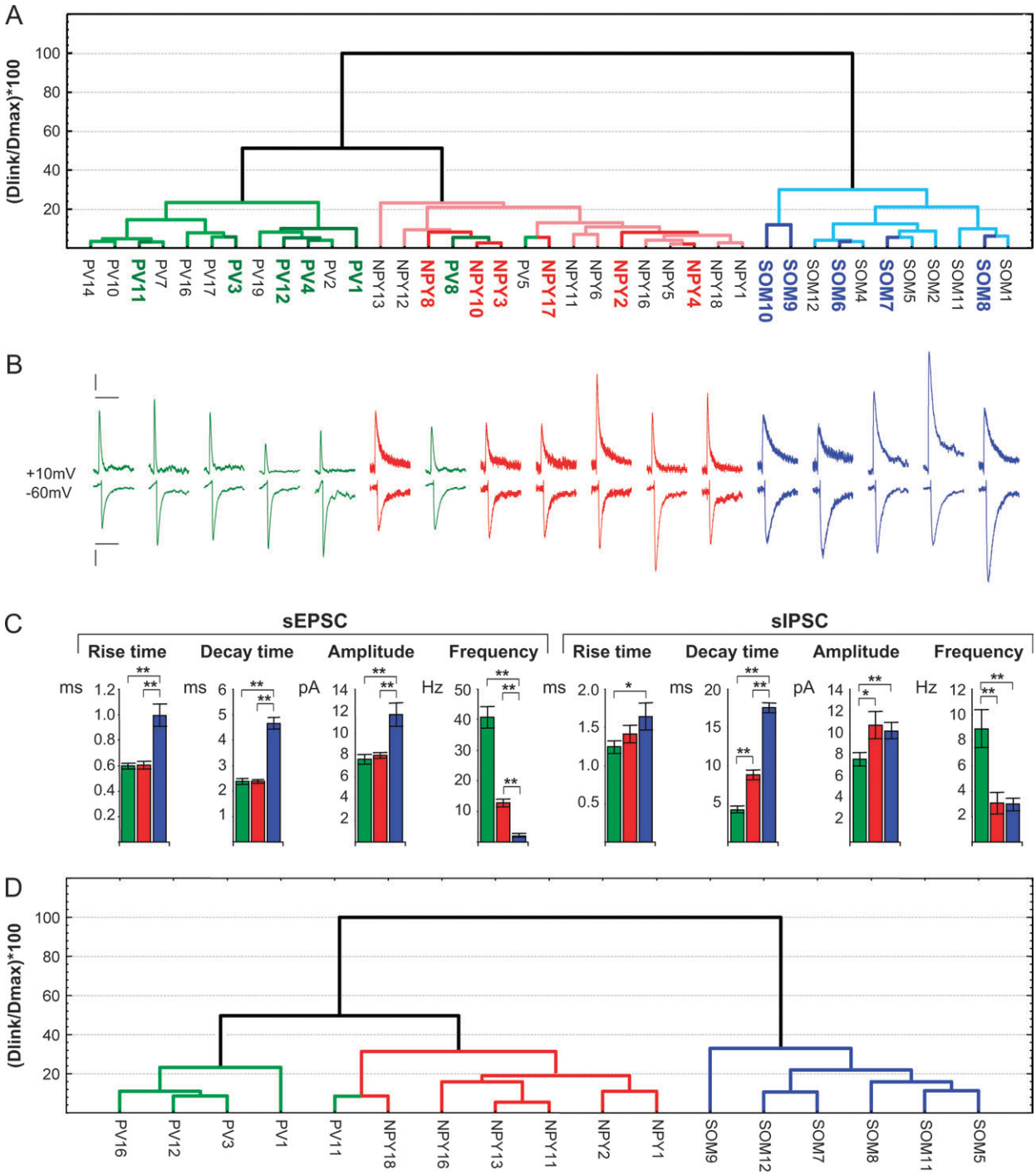

Figure 3. Physiological cluster analysis. (*A*) Cluster analysis tree of 8 variables describing the spontaneous PSCs for 39 cells: 14 PV, 14 NPY, and 11 SOM. The 18 cells that were reconstructed are represented in darker colors and colored cell names. (*B*) EPSC and IPSC averages for each reconstructed neuron in the order in which they appear in the cluster analysis tree. Each average is composed of about 300 spontaneous PSCs. Scale bars: for IPSC averages, 2 pA and 60 ms; for EPSC averages, 2 pA and 15 ms. (*C*) Pooled data of the 8 variables used in the cluster analysis represented as averages for each cell group. Statistical significance assessed by *t*-test; $*P < 0.05$, $**P < 0.01$. (*D*) Cluster analysis tree of 8 variables describing the miniature PSCs for a subset of cells: 5 PV, 6 NPY, and 6 SOM.

Tile Centroid Distance from the Soma

To describe the dendritic and axonal arbors, we used tiling analysis of the 2-dimensional projection of the neurons. Thus, this tiling was performed arbitrarily in the coronal plane of the slice, and this fact should be kept in mind as a potential limitation of topological analysis which relies on tiling. Two tiles were drawn on each cell to encompass the dendrites and axon, respectively (Fig. 6). Several parameters were computed for each tile (see Supplementary Table 1), including the center of gravity, or "tile centroid," defined by its distance from the center of gravity of the soma. Interestingly, both the dendritic and axonal tile centroids arose as important morphological predictors of each cell class. Figure 5 shows a schematic diagram of these 2 variables for each cell type. SOM cells

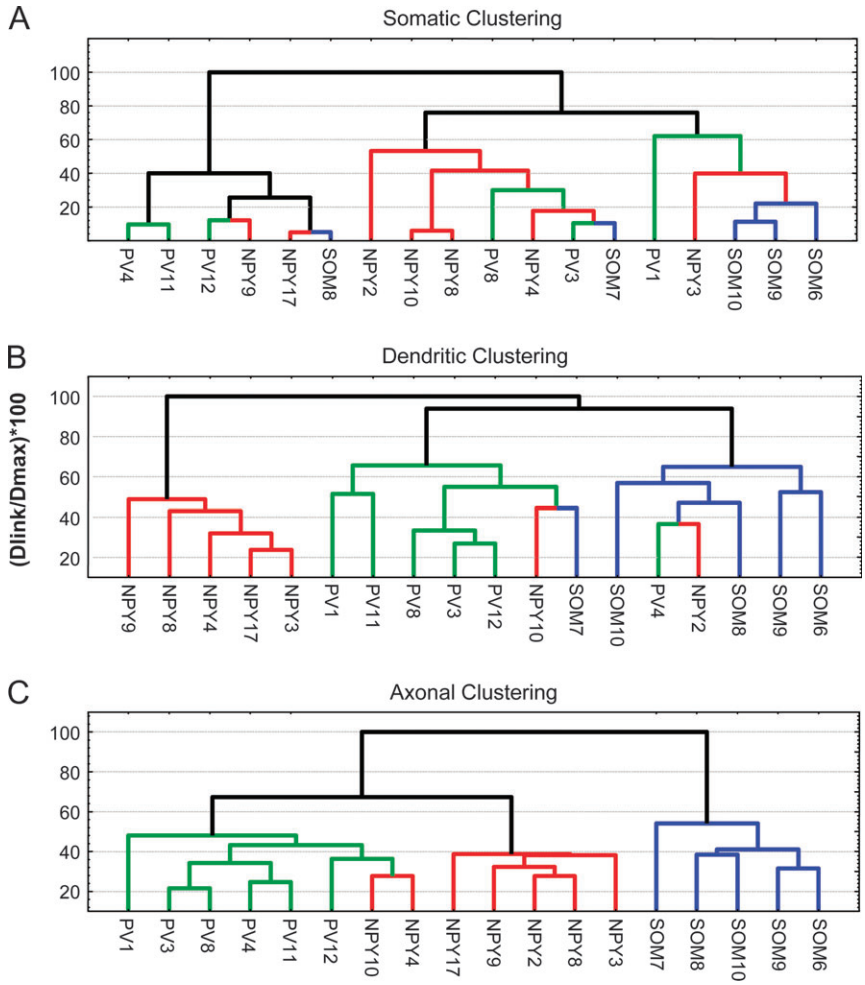

Figure 4. Cluster analysis of morphologies of somata, dendrites, and axons. (*A*) Cluster analysis tree of the 18 reconstructed cells using only the 4 variables that described size, shape, and location of the somata. (*B*) Cluster analysis tree of the 18 reconstructed neurons using only the 25 variables pertaining to the dendrites, including the 2 variables that describe the relationship between dendrites and axon. (*C*) Cluster analysis tree of the 18 reconstructed neurons using only the 34 variables pertaining to the axon, including the 2 variables that describe the relationship between axon and dendrites.

presented the most skewed axonal and dendritic arbors, whereas NPY cells distributed their processes the most evenly.

Intuitively, this skewness could be related to the total length of the cell's processes or to the area of the tile, because a longer process with a greater surface area allows for a greater variability in the exact position of the resulting centroid. However, an examination of the relationship between total process length, tile area, and tile centroids showed little or no correlation. The dendritic centroid distance from the soma for the pooled data was 21% inversely correlated with the total dendritic length and 8% inversely correlated with the dendritic tile area, whereas the axonal centroid location was 28% inversely correlated with the total axonal length and 40% correlated with the axonal tile area. Thus, we conclude that the locations of the dendritic and axonal tile centroids are independent morphological characteristics, arising perhaps from developmental factors regulating the overall appearance of a cell and not as epiphenomena of other parameters, such as process length and tile area.

Fractal Dimensionality of Axon

Fractal dimensionality is another type of tiling analysis that measures a 1-dimensional axon's ability to fill a 2-dimensional space. A score close to 1 implies that the axon fills the space poorly, whereas a score close to 2 implies that the axon fills the space almost entirely (Fig. 6*A*). Whereas the axons of PV cells filled their tile almost entirely, the axons of SOM cells left a significant portion of their tile empty. Specifically, PV cells had axons of the highest dimensionality with an average of 1.45 ± 0.02 fractal units as compared with NPY axons (1.37 ± 0.03 fractal units) and SOM cells, which appeared as the most unidimensional (1.32 ± 0.02 fractal units) (Fig. 6*B*).

We reasoned that, based on the definition of fractal dimensionality, this measure should correlate with a measure of "axonal density," which we computed by dividing the total axonal length by the axonal tile area. Indeed, this new variable proved 67% correlated with fractal dimensionality. Figure 6*C* shows that this new variable maintained the relationship between the 3 groups of cells, though reducing the difference between PV and NPY cells. Thus, the axonal density can be used to predict interneurons subtype.

Axonal Bifurcations

An axonal bifurcation can be classified into 3 categories: primary bifurcations give rise to 2 ending segments, secondary bifurcations give rise to 1 ending segment and 1 segment which

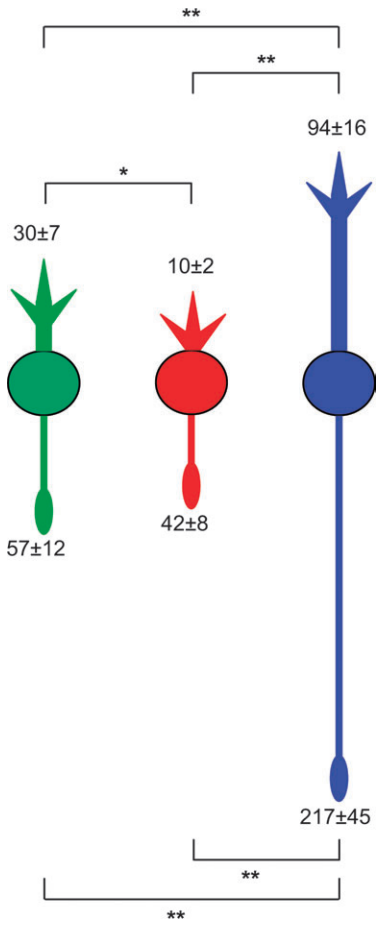

Figure 5. Dendritic and axonal tile centroid distances from the soma. The location of the tile centroid of axons and dendrites was established using NeuroExplorer. A group average was computed and used for the graphical representation. Statistical significance using *t*-test; $*P < 0.05$, $**P < 0.01$.

bifurcates into 2 new segments, and a tertiary bifurcation gives rise to 2 segments each of which gives rise to 2 additional segments. The relative amount of each type of bifurcation can be considered a measure of the lopsidedness of the cells axon. The more secondary bifurcations, the more lopsided the axon is. This concept is similar to the "partition asymmetry" introduced by van Pelt and others (1997).

Following the initial cross-correlation matrix on the 98 morphological variables, only one of the 3 bifurcation measures remained because the 3 variables were intercorrelated by more than 80%. Percentage of primary bifurcations was chosen to be representative because this variable was most correlated with both the other two.

Figure 7*A* outlines the relative amounts of the 3 different types of bifurcations and the small fraction of trifurcations for each neurochemical group. The most obvious difference between the 3 groups is that SOM cells contained the most secondary bifurcations and were therefore the most lopsided. The main difference between PV and NPY cells was the higher fraction of trifurcations for the latter.

To further characterize the lopsidedness, we examined the distribution of axonal segments by branch order. We reasoned that the cumulative distribution of axonal segments (as defined by number per branch order) would show a steeper rise for more symmetrical cells and a more moderate one for more lopsided cells. As can be seen in Figure 7*B*, this cumulative distribution does indeed roughly cluster the cells by neurochemical content and reveals NPY cells to be most symmetric and SOM cells most lopsided.

Next we divided each cell's axon into 2 at the 1st branch point and measured the length of the resulting pieces. Two averages were computed for each cell type: the average of the shorter piece and the average of the longer piece. For cells with 2 putative axons, the measure was established for each axon individually and then a cell average was computed prior to entering the data into the pooled group. Figure 7*C* is a graphic representation of this measure and clearly shows the principle described above: NPY cells have the most symmetrical axons, whereas SOM cells have the most lopsided axons.

One possibility for this difference between cell types could be due to an artifact during the processing. For example, axons projecting over long distances or axons of high total length might be more prone to cutting. To examine this issue, we analyzed whether or not percent primary bifurcations correlated with total axonal length or axonal tile area. We found only a 28% correlation with total length and a 43% inverse correlation with tile area, whereas the correlation with neurochemical content was 84%.

Axonal Sholl

Finally, we computed the Sholl variable, defined as the percent length of process in 100 μm concentric circles. Because of the large degree of correlation within Sholl measures of axons, only 3 out of the original 10 variables remained after the cross-correlation matrix. Therefore, it can be inferred that the individual Sholl variable that was detected by the PCA as a significant parameter in the classification of these cells was representative of the entire axonal Sholl. Figure 8 shows the cumulative distribution of the axonal length as a function of distance from the cell body for each reconstructed cell as well as for group averages. As demonstrated both graphically in Figure 8*A,B* as well as quantitatively in Figure 8*C*, the axonal Sholl varied significantly between the groups at several distances from the cell body, with the greatest difference being between NPY and SOM cells and the least difference between PV and NPY cells.

Discussion

Existence of Distinct Classes of Neocortical Interneurons

Are there separate classes of neocortical interneurons? One view holds that there are specific subgroups of "short axon" cells with specific morphological and electrophysiological characteristics (Ramón y Cajal 1899; Lorente de No 1922 [reprinted 1992]; Fairen and others 1984; Gonchar and Burkhalter 1997; Kawaguchi and Kubota 1997; Somogyi and others 1998; Gupta and others 2000; Markram and others 2004), whereas an opposite view highlights a potential continuum of cells morphologies, each perhaps endowed with a unique combination of electrophysiological properties (Parra and others 1998). This issue is of great importance. If there are indeed subtypes of neocortical interneurons, it is likely that each type could play a specific role in the circuit. Therefore, as a 1st step towards understanding of any circuit it becomes necessary to define its individual elements.

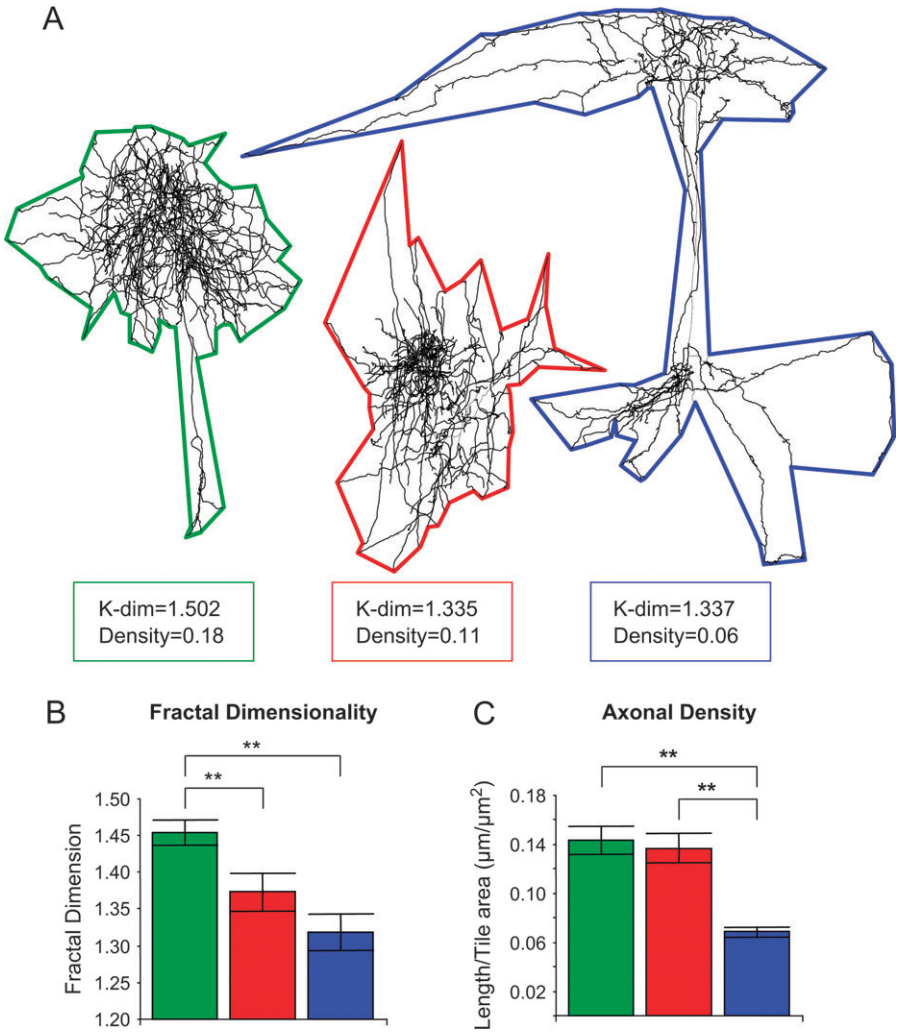

Figure 6. Axonal fractal dimensionality differences between groups. (*A*) Examples of axons and their tiles from each cell group. Notice the varying amount of "empty space" inside the tile. (*B*) Averages of fractal dimensionality for each group. (*C*) Averages of "axonal density" for each group. This variable was established by dividing an axon's total length by its tile area. Statistical significance using *t*-test; $*P < 0.05$, $**P < 0.01$.

The controversy is partly due to the use of qualitative criteria to generate classifications of neurons. Unfortunately, criteria that are important and clear to one investigator may seem arbitrary to another. An ultimate solution to this dispute could be to use the internal description that each cell has of itself (Yuste 2005), that is, its transcriptional specification (Anderson and others 1997) or the pattern of expression of all its genes (Monyer and Markram, 2004). Thus, systematic efforts with techniques such as single-cell polymerase chain reaction (Cauli and others 1997, 2000; Wang and others 2002; Toledo-Rodriguez and others 2004), microarrays (Zhang and others 2001), or developmental studies identifying the transcriptional fate plan (Anderson and others 1997) appear ideal to provide an ultimate classification.

To explore this issue, we used cluster analysis (Cauli and others 1997, 2000; Kozloski and others 2001; Tsiola and Yuste 2003; Krimer and others 2005) of morphological and electrophysiogical variables of 3 groups of neocortical interneurons, defined as expressing 3 different genes: PV, SOM, or NPY. The cluster analysis was blind to the identity of the cell, yet neurons still clustered into these 3 groups based on their morphological and physiological parameters. We made no assumptions as to which variable was more or less important, and let the algorithm identify in multidimensional space whether or not cells could be segregated into significant clusters. Our results indicate that each of the 3 groups of interneurons studied is also distinguished by a constellation of morphological and electrophysiological characteristics and the fact that these 3 clusters match subpopulations of interneurons, as defined by known cellular markers, confirms the validity of the method. Our data demonstrate that there are indeed distinct classes of neocortical interneurons and are also consistent with a recent study that has also applied cluster analysis of morphological and physiological features to separate 2 different types of neocortical interneurons (Krimer and others 2005). At the same time, we should caution the reader that all our data come from juvenile animals, and it is possible that further developmental differences (or similarities) could arise among these studied groups of interneurons in the mature circuit. We also would like to further limit our conclusions to the specific cortical area and species used because there are major differences in cell morphologies across different cortical areas or species (DeFelipe and others 2002).

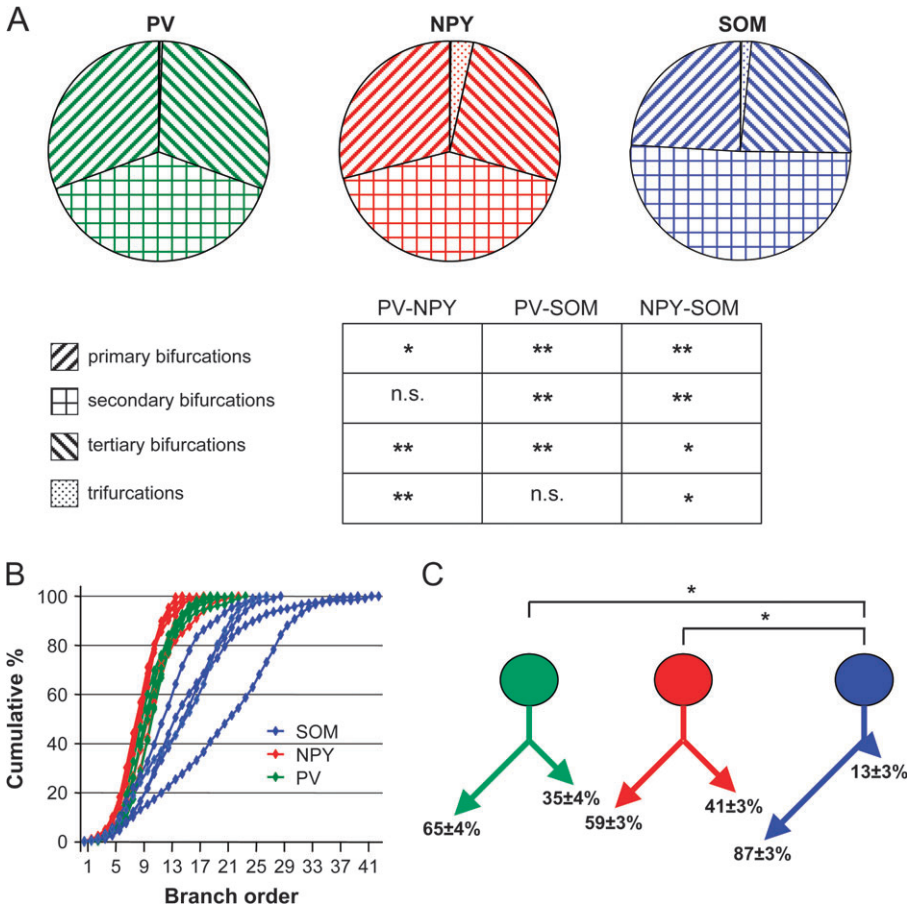

Figure 7. Axonal bifurcation differences between groups. (*A*) Graphical representation of the average distribution or primary, secondary, tertiary bifurcations and trifurcations for each group. (*B*) Cumulative distribution of branches by branch order for each cell. The steeper the curve, the more evenly distributed the branches of the axon are by branch order. (*C*) For each cell, the axon was split into 2 at its 1st node. An average of the longest versus the shortest piece was computed for each group and is represented graphically here. Statistical significance using *t*-test; $*P < 0.05$, $**P < 0.01$.

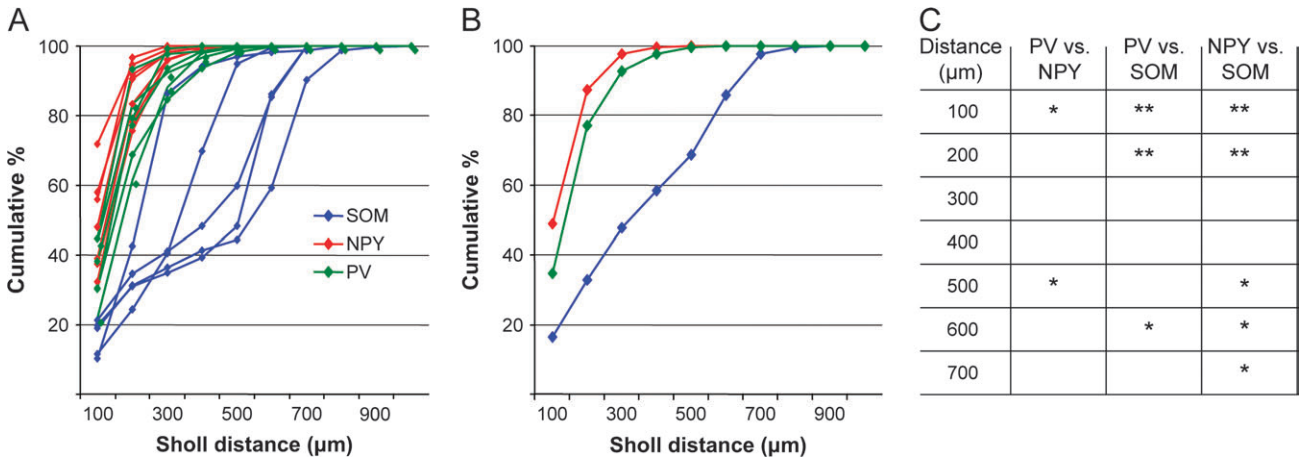

Figure 8. Axonal Sholl length differences between groups. (*A*) Cumulative distribution of the axonal length of each cell as defined by measuring the percentage of the total arbor in each 100 μm concentric circle starting from the soma. (*B*) For each concentric circle, a group average was calculated. Cumulative distribution of axonal length by group average was then plotted. (*C*) Statistical analysis of group average Sholl indicating highly significant differences between groups in many of the concentric circles. Statistical significance using *t*-test; $*P < 0.05$, $**P < 0.01$.

Are the groups we identify in this study separated by sharp boundaries, or do they represent peaks in an otherwise continuum space of morphological or electrophysiological variance? Given the highly selected nature of our sample, where neurons were targeted and studied only if they expressed GFP in 3 different mouse strains, we cannot rule out that a wider sample, such as a large randomized characterization of interneurons, could result in less sharp distinctions. Nevertheless, an

overall consideration of our dataset, particularly in relation with the peculiar axonal morphologies that are characteristic for each cell class, makes it simpler to assume that each class explores a relatively narrow subset of phenotypic variability.

Although based on a reduced sample of neurons from a specific neocortical area, our results are consistent with the increasingly more complete molecular understanding of neuronal differentiation in other parts of the central nervous system (CNS), which is providing strong evidence for the existence of different functional neuronal cells types. For example, in the spinal cord, different population of motoneurons, sensory neurons, and interneurons appeared to be specified by one or a specific set of transcription factors whose expression is controlled by a different combination of inducer molecules, set up by the neuron's coordinate in anteroposterior and dorsoventral axes (Lee and Jessell 1999; Jessell 2000; Dasen and others 2005). These transcription factors specify not only the morphological features of the axon and dendrites but also the precise synaptic connectivity. Moreover, the axonal morphology in the spinal cord is not only a predictor of the neuronal identity, as it reflects the choice of transcription factors that the neuron expresses, but also of neuronal function because it determines the targets that the neuron contacts.

Correlation between Morphological and Physiological Parameters

In our quantitative analysis, we uncovered a systematic relationship between electrophysiological and morphological parameters, along the independent parameter defined by the neurochemical content. We then used the correlation matrix to explore which are the key variables that can be best used to define each cell group. We encounter that the morphological variables associated with the axonal arborization have the highest correlation with the physiological variables that cluster the different interneuron classes. Lorente de No (1922) presciently proposed that axonal morphology is the most important parameter in the classification of cortical neurons. More than 80 years later, we are able to offer quantitative evidence for his intuition.

We have detected that several aspects of the axonal morphology are differentially correlated with the 3 types of interneurons. The differences in dendritic and axonal centroid distances from the soma, as well as the difference in ratio of bifurcation type could be related to differential sampling and/or innervation of specific cortical sublamina. Whereas the more compact, symmetrical NPY cells are likely to function within specific laminar or sublaminar microcircuits, the more skewed and broadly branching SOM cells would monitor or exert their influence over a larger territory. The differences in fractal dimensionality could also have implications to the local connectivity. The higher dimensional axons of PV cells could enable them to target more proximal dendrites of local cells, whereas the lower dimensional SOM cells may target cells farther away. Even if the overall number of postsynaptic cells might be equal for a PV and SOM cell, the target zone will vary significantly. Finally, the differences in bifurcation are quite intriguing because in mammalian neurons the exact morphology of the axonal arbor is not thought to matter, other than in different delays caused by axons of different lengths or widths. Nevertheless, in invertebrates it has been demonstrated that different branches of an axon can respond preferentially to action potential trains of different frequencies (Debanne 2004), so it is possible that in neocortical interneurons different branching patterns could have a physiological impact.

In addition to morphological predictors, our study points out a difference in physiological parameters among the 3 different types of neocortical interneurons studied, and we could speculate about the meaning of these findings. Interneurons in hippocampus are thought to fine-tune the cortical network activity, thus molding it into meaningful information (Somogyi and others 1998). The precise, submillisecond, firing time of an interneuron could therefore be a very important part of the cell's role in the network. Pouille and Scanziani (2001) showed that the subcellular location of GABAergic synapses onto a principal cell can have different effects on the subsequent firing of the principal cells, acting to optimize coincidence detection in the soma, but allowing a broader integration window in the dendrites. Combining this principle with our finding that SOM cells, which target distal apical dendrites, receive PSCs with slower kinetics than PV cells, which target somas, we could infer that the differentiation of average kinetics between different classes of interneurons provides the cortex with a method of elongating the overall window of temporal summation.

Correlation between Input Kinetics and Axonal Morphology

In addition to uncovering specific morphological and physiological characteristic of different interneuron classes, our results also show that the postsynaptic target of an interneuron correlates with the kinetics of synaptic inputs. These data are consistent and confirm similar earlier findings in hippocampus (Cossart and others, 2006). In both systems, the correlation between axonal topology and synaptic temporal characteristics is strong and is therefore likely to apply also to other parts of the CNS. What is the functional significance of this intriguing correlation? Why would the kinetics of synaptic input in the somata or dendrites of an interneuron be correlated with the specific properties of its axonal morphology?

Neocortical interneurons appear to target different regions of the pyramidal neuron's dendritic tree. PV neurons target somata or proximal dendrites, whereas SOM cells are thought to preferentially contact distal dendrites (Fairen and others 1984; Somogyi and others 1998). Less is known about the specific targets of NPY neurons, although they could correspond to the neurogliaform cells, which are known to target spines (Tamas and others 2003). Therefore, there be a functional logic, by which interneurons with faster synaptic current kinetics contact somata, whereas those with slower kinetics contact dendrites or spines. This system of parallel channels seems designed to carry our processing of temporal information at different temporal frequencies and would generally agree with the finding that different classes of hippocampal interneurons are preferentially activated at different temporal phases of the network oscillations in vivo (Klausberger and others 2003). Thus, each interneuron class would have, as its signature, particular temporal properties, which could play an important role for oscillations or for more complex temporal patterning (Ikegaya and others 2004).

Supplementary Material

Supplementary material can be found at http://www.cercor.oxfordjournals.org/

Notes

We thank J. Friedman for his gift of NPY mice and J. Goldberg and F. Hamzei-Sichani for comments. This work was funded by the National Eye Institute and the National Institute of Neurological Diseases.

Address correspondence to Rafael Yuste, Howard Hughes Medical Institute, Department of Biological Sciences, Columbia University, 1212 Amsterdam Avenue, Box 2435, New York, NY 10027, USA. rmy5@columbia.edu.

References

Anderson S, Eisenstat D, Shi L, Rubenstein J. 1997. Interneuron migration from basal forebrain to neocortex: dependence on Dlx genes. Science 278:474–476.

Baraban SC, Tallent MK. 2004. Interneuron diversity series: interneuronal neuropeptides—endogenous regulators of neuronal excitability. Trends Neurosci 27:135–142.

Cossart R, Dumitriu D, Petanjek Z, Hirsch JC, Ben-Ari Y, Esclapez M, Bernard C. 2006. A kinetic signature for interneurons. Hippocampus. Forthcoming.

Cauli B, Audinat E, Lambolez B, Angulo MC, RopertN, Tsuzuki K, Hestrin S, Rossier J. 1997. Molecular and physiological diversity of cortical nonpyramidal cells. J Neurosci 17:3894–3906.

Cauli B, Porter JT, Tsuzuki K, Lambolez B, Rossier J, Quenet B, Audinat E. 2000. Classification of fusiform neocortical interneurons based on unsupervised clustering. Proc Natl Acad Sci USA 97:6144–6149.

Dasen J, Tice B, Brenner-Morton S, Jessell T. 2005. A hox regulatory network establishes motor neuron pool identity and target-muscle connectivity. Cell 123:477–491.

Debanne D. 2004. Information processing in the axon. Nat Rev Neurosci 5:304–316.

DeFelipe J, Elston GN, Fujita I, Fuster J, Harrison KH, Hof PR, Kawaguchi Y, Martin KAC, Rockland KS, Thomsom AM, Wang SS, White El, Yuste R. 2002. Neocortical circuits: evolutionary aspects and specificity versus non-specificity of synaptic connections. Remarks, main conclusions and general comments and discussion. J Neurocytol 31:387–416.

Esclapez M, Hirsch JC, Khazipov R, Ben-Ari Y, Bernard C. 1997. Operative GABAergic inhibition in hippocampal CA1 pyramidal neurons in experimental epilepsy. Proc Natl Acad Sci USA 94: 12151–12156.

Fairen A, De Felipe J, Regidor J. 1984. Nonpyramidal neurons. In: Peters A, Jones EG, editors. Cerebral cortex. New York: Plenum. p 201–253.

Freund TF, Buzsaki G. 1996. Interneurons of the hippocampus. Hippocampus 6:347–470.

Gonchar Y, Burkhalter A. 1997. Three distinct families of GABAergic neurons in the rat visual cortex. Cereb Cortex 7:347–358.

Gupta A, Wang Y, Markram H. 2000. Organizing principles for a diversity of GABAergic interneurons and synapses in the neocortex. Science 287:273–278.

Ikegaya Y, Aaron G, Cossart R, Aronov D, Lampl I, Ferster D, Yuste R. 2004. Synfire chains and cortical songs: temporal modules of cortical activity. Science 304:559–564.

Jessell TM. 2000. Neuronal specification in the spinal cord: inductive signals and transcriptional codes. Nat Rev Genet 1:20–29.

Jonas P, Bischofberger J, Fricker D, Miles R. 2004. Interneuron diversity series: fast in, fast out—temporal and spatial signal processing in hippocampal interneurons. Trends Neurosci 27:30–40.

Kawaguchi Y, Kubota Y. 1997. GABAergic cell subtypes and their synaptic connections in rat frontal cortex. Cereb Cortex 7: 476–486.

Klausberger T, Magill P, Marton L, Roberts J, Cobden P, Buzsaki G, Somogyi P. 2003. Brain-state- and cell-type-specific firing of hippocampal interneurons in vivo. Nature 421:844–848.

Kozloski J, Hamzei-Sichani F, Yuste R. 2001. Stereotyped position of local synaptic targets in neocortex. Science 293:868–872.

Krimer L, Zaitsev A, Czanner G, Kroner S, Gonzalez-Burgos G, Povysheva N, Iyengar S, Barrionuevo G, Lewis D. 2005. Cluster analysis-based physiological classification and morphological properties of inhibitory neurons in layers 2-3 of monkey dorsolateral prefrontal cortex. J Neurophysiol 94:3009–3022.

Lee K, Jessell T. 1999. The specification of dorsal cell fates in the vertebrate central nervous system. Annu Rev Neurosci 22:261–294.

Lorente de No R. 1922 (reprinted 1992). The cerebral cortex of the mouse (a first contribution—the "acoustic" cortex). Somatosens Mot Res 9:3–36.

Maccaferri G, Lacaille JC. 2003. Interneuron diversity series: hippocampal interneuron classifications—making things as simple as possible, not simpler. Trends Neurosci 26:564–571.

Markram H, Toledo-Rodriguez M, Wang Y, Gupta A, Silberberg G, Wu C. 2004. Interneurons of the neocortical inhibitory system. Nat Rev Neurosci 5:793–807.

Monyer H, Markram H. 2004. Interneuron diversity series: molecular and genetic tools to study GABAergic interneuron diversity and function. Trends Neurosci 27:90–97.

Mott DD, Dingledine R. 2003. Interneuron diversity series: interneuron research—challenges and strategies. Trends Neurosci 26:484–488.

Oliva AA Jr, Jiang M, Lam T, Smith KL, Swann JW. 2000. Novel hippocampal interneuronal subtypes identified using transgenic mice that express green fluorescent protein in GABAergic interneurons. J Neurosci 20:3354–3368.

Parra P, Gulyas AI, Miles R. 1998. How many subtypes of inhibitory cells in the hippocampus? Neuron 20:983–993.

Pouille F, Scanziani M. 2001. Enforcement of temporal fidelity in pyramidal cells by somatic feed-forward inhibition. Science 293:1159–1163.

Ramón y Cajal S. 1899. La Textura del Sistema Nerviosa del Hombre y los Vertebrados. Primera Edicion. Madrid: Moya.

Roseberry A, Liu H, Jackson A, Cai X, Friedman J. 2004. Neuropeptide Y-mediated inhibition of proopiomelanocortin neurons in the arcuate nucleus shows enhanced desensitization in ob/ob mice. Neuron 41:711–722.

Somogyi P, Tamas G, Lujan R, Buhl E. 1998. Salient features of synaptic organisation in the cerebral cortex. Brain Res Brain Res Rev 26:113–135.

Sterling P. 1990. Retina. In: Shepherd GM, editors. The synaptic organization of the Brain. Oxford: Oxford University Press.

Tamas G, Lorincz A, Simon A, Szabadics J. 2003. Identified sources and targets of slow inhibition in the neocortex. Science 299:1902–1905.

Toledo-Rodriguez M, Blumenfeld B, Wu C, Luo J, Attali B, Goodman P, Markram H. 2004. Correlation maps allow neuronal electrical properties to be predicted from single-cell gene expression profiles in rat neocortex. Cereb Cortex 14:1310–1327.

Tsiola A, Yuste R. 2003. Classification of neurons in the mouse primary visual cortex. J Comp Neurol 461:415–428.

van Pelt J, Dityatev A, Uylings H. 1997. Natural variability in the number of dendritic segments: model-based inferences about branching during neurite outgrowth. J Comp Neurol 387, 325–340.

Wang Y, Gupta A, Toledo-Rodriguez M, Wu CZ, Markram H. 2002. Anatomical, physiological, molecular and circuit properties of nest basket cells in the developing somatosensory cortex. Cereb Cortex 12:395–410.

Yang XW, Model P, Heintz N. 1997. Homologous recombination based modification in Escherichia coli and germline transmission in transgenic mice of a bacterial artificial chromosome. Nat Biotechnol 15:859–865.

Yuste R. 2005. Origin and classification of neocortical interneurons. Neuron 48:524–527.

Zhang H, Yu CY, Singer B, Xiong M. 2001. Recursive partitioning for tumor classification with gene expression microarray data. Proc Natl Acad Sci USA 98:6730–6735.